Cathodo- and photoluminescence in Yb^{3+}-Er^{3+} co-doped PbF_2 nanoparticles

V. K. Tikhomirov[1*], G. Adamo[2], A. E. Nikolaenko[2], V. D. Rodriguez[3], P. Gredin[4], M. Mortier[4], N. I. Zheludev[2], and V. V. Moshchalkov[1,5]

[1] *INPAC – Institute for Nanoscale Physics and Chemistry, Catholic University Leuven, Belgium*
[2] *Optoelectronics Research Centre, University of Southampton, Southampton SO17 1BJ, UK*
[3] *Departamento de Física Fundamental y Experimental, Electrónica y Sistemas, Universidad de La Laguna, Tenerife, Spain.*
[4] *Laboratoire de Chimie de la Matière Condensée, Ecole Nationale Supérieure de Chimie de Paris, UPMC – Paris 6 - CNRS UMR7574, France*
[5] *Victor.Moshachalkov@fys.kuleuven.be*
[*] *Victor.Tikhomirov@fys.kuleuven.be*

Abstract: We have prepared and studied the PbF_2:(Yb^{3+},Er^{3+}) co-doped nanoparticles, with chemical formula $(Yb\text{-}Er)_xPb_{1-x}F_{2+x}$, where $x = 0.29$, $Yb^{3+}/Er^{3+} = 6$, and estimated the energy efficiency for their cathodoluminescence, mostly of Yb^{3+}, and up-conversion photoluminescence of Er^{3+} to reach more than 0.5% and 20%, respectively, which may be the highest to date for *rare-earth doped nanoparticles*. Electron beam induced temperature rise in the nanoparticles has been estimated by measuring the ratio of green emission bands of Er^{3+}. These high efficiencies are due to high doping level of nanoparticles and due to low phonon energy of the PbF_2 host.

©2010 Optical Society of America

OCIS codes: (160.5690) Rare earth doped materials; (160.4236) Nanomaterials, (250.5230) Photoluminescence

---

References and links

1. L. Aigouy, P. Lalanne, J. P. Hugonin, G. Julié, V. Mathet, and M. Mortier, "Near-field analysis of surface waves launched at nanoslit apertures," Phys. Rev. Lett. **98**(15), 153902 (2007).
2. E. Plum, V. A. Fedotov, P. Kuo, D. P. Tsai, and N. I. Zheludev, "Towards the lasing spaser: controlling metamaterial optical response with semiconductor quantum dots," Opt. Express **17**(10), 8548–8551 (2009).
3. H. Zhou, M. Wissinger, J. Fallert, R. Hauschild, F. Stelzl, C. Klingshirn, and H. Kalt, "Ordered, uniform-sized ZnO nanolaser arrays," Appl. Phys. Lett. **91**(18), 181112 (2007).
4. P. Salas, C. Angeles-Chavez, J. A. Montoya, E. De la Rosa, L. A. Diaz-Torres, H. Desirena, A. Martinez, M. A. Romero-Romo, and J. Morales, "Synthesis, characterization and luminescence properties of ZrO_2:Yb^{3+}-Er^{3+} nanophosphor," Opt. Mater. **27**(7), 1295–1300 (2005).
5. D. Matsuura, "Red, green and blue up-conversion luminescence of trivalent rare earth ion-doped Y_2O_3 nanocrystals," Appl. Phys. Lett. **81**(24), 4526–4528 (2002).
6. J. Zhang, Y. Fu, and J. R. Lakowicz, "Luminescent images of single gold nanoparticles and their labeling on silica beads," Opt. Express **15**(20), 13415–13420 (2007).
7. J. J. Mock, S. J. Oldenburg, D. R. Smith, D. A. Schultz, and S. Schultz, "Composite plasmon resonant nanowires," Nano Lett. **2**(5), 465–469 (2002).
8. E. Beaurepaire, V. Buissette, M.-P. Sauviat, D. Giaume, K. Lahlil, A. Mercuri, D. Casanova, A. Huignard, J.-L. Martin, T. Gacoin, J.-P. Boilot, and A. Alexandrou, "Functionalized fluorescent oxide nanoparticles: artificial toxins for sodium channel targeting and imaging at the single molecule level," Nano Lett. **4**(11), 2079–2083 (2004).
9. V. K. Tikhomirov, K. Driesen, V. D. Rodriguez, P. Gredin, M. Mortier, and V. V. Moshchalkov, "Optical nanoheater based on the Yb^{3+}-Er^{3+} co-doped nanoparticles," Opt. Express **17**(14), 11794–11798 (2009).
10. V. K. Tikhomirov, L. F. Chibotaru, D. Saurel, P. Gredin, M. Mortier, and V. V. Moshchalkov, "$Er^{(3+)}$-doped nanoparticles for optical detection of magnetic field," Nano Lett. **9**(2), 721–724 (2009).
11. M. Mortier, and G. Patriarche, "Oxide glass used as inorganic template for fluorescent fluoride nano-particle synthesis," Opt. Mater. **28**(12), 1401–1404 (2006).
12. Z.-L. Wang, H. L. W. Chan, H.-L. Li, and J. H. Hao, "Highly efficient low-voltage cathodoluminescence of LaF_3:Ln^{3+} ($La=Eu^{3+}$, Ce^{3+}, Tb^{3+}) spherical particles," Appl. Phys. Lett. **93**, 141106 (2008).
13. J. Hao, S. A. Studenkin, and M. Cocivera, "Blue, green and red cathodoluminescence of Y_2O_3 phosphor films prepared by spray pyrolysis," J. Lumin. **93**(4), 313–319 (2001).

14. N. Rakov, F. E. Ramos, G. Hirata, and M. Xiao, "Strong photoluminescence and cathodoluminescence due to f-f transitions in Eu^{3+}-doped powders prepared by direct combustion synthesis and thin films deposited by laser ablation," Appl. Phys. Lett. **83**(2), 272–274 (2003).
15. L. Aigouy, G. Tessier, M. Mortier, and B. Charlot, "Scanning thermal imaging of microelectronic circuits with a fluorescent nanoprobe," Appl. Phys. Lett. **87**(18), 184105 (2005).
16. T. Hayakawa, M. Hayakawa, and M. Nogami, "Estimation of the fs laser spot temperature inside TeO_2-ZnO-Nb_2O_5 glass by using up-conversion green fluorescence of Er^{3+} ions," J. Alloy. Comp. **451**(1–2), 77–80 (2008).
17. T. Welker, "Recent developments on phosphors for fluorescent lamps and cathode-ray tubes," J. Lumin. **48–49**, 49–56 (1991).
18. G. Adamo, K. F. MacDonald, Y. H. Fu, C. M. Wang, D. P. Tsai, F. J. de Abajo, and N. I. Zheludev, "Light well: a tunable free-electron light source on a chip," Phys. Rev. Lett. **103**(11), 113901 (2009).
19. F. Auzel, "Up-conversion and anti-Stokes processes with d and f ions in solids," Chem. Rev. **105**(1), 139–174 (2004).
20. V. K. Tikhomirov, K. Driesen, C. Görller-Walrand, and M. Mortier, "Broadband telecommunication wavelength emission in $Yb^{(3+)}$-$Er^{(3+)}$-$Tm^{(3+)}$ co-doped nano-glassceramics," Opt. Express **15**(15), 9535–9540 (2007).
21. V. K. Tikhomirov, D. Furniss, I. M. Reaney, M. Beggiora, M. Ferrari, M. Montagna, and R. Rolli, "Fabrication and characterization of nanoscale, Er^{3+}-doped, ultratransparent oxyfluoride glass-ceramics," Appl. Phys. Lett. **81**(11), 1937–1939 (2002).
22. V. D. Rodríguez, V. K. Tikhomirov, J. Méndez-Ramos, J. del-Castillo, and C. Görller-Walrand, "Measurement of quantum yield of up-conversion Luminescence in $Er^{(3+)}$-doped nano-glass-ceramics," J. Nanosci. Nanotechnol. **9**(3), 2072–2075 (2009).
23. V. D. Rodríguez, V. K. Tikhomirov, J. Méndez-Ramos, and A. B. Seddon, "The shape of the 1.55 μm emission band of the Er^{3+} dopant in oxyfluoride nano-scaled glass-ceramics," Europhys. Lett. **69**(1), 128–134 (2005).
24. J. Fallert, R. J. B. Dietz, J. Sartor, D. Schneider, C. Klingshirn, and H. Kalt, "Co-existence of strongly and weakly localised random laser modes," Nat. Photonics **3**(5), 279–282 (2009).
25. J. F. Suyver, M. K. van Veen, D. Biner, K. W. Krämer, and H. U. Güdel, "Upconversion spectroscopy and properties of $NaYF_4$ doped with Er^{3+}, Tm^{3+} and/or Yb^{3+}," J. Lumin. **117**(1), 1–12 (2006).
26. D. J. M. Bevan, J. Strähle, and O. Greis, "The crystal-structure of tveitite, an ordered yttrofluorite mineral," J. Solid State Chem. **44**(1), 75–81 (1982).
27. S. Hull, "Superionic crystal structures and conduction processes," Rep. Prog. Phys. **67**(7), 1233–1314 (2004).

1. Introduction

The luminescent *nanoparticles* have been attracting recently an interest in nano-scale optics and photonics, for instance in plasmon near-field microscopy [1,2], nanolasers [2,3], nanophosphors [4,5], nanolabels [6–8] and nanosensors [9,10]. Rare-earth doped nanoparticles could be of particular importance since the rare-earth ions are well known as source of efficient luminescence, especially when doped in a host which has low phonon energy and capable of high doping level, such as ionic fluoride PbF_2-based nanoparticles [11].

While the photoluminescence (PL) of rare-earth dopants has been a subject of intense investigations for decades, the reports about their cathodoluminescence (CL) are scarce, e.g. in [12–14]. To our knowledge, CL of rare-earth doped *nanoparticles* has not been reported to date and little has been reported about PL of rare-earth doped *nanoparticles*, e.g. in [9–11], in particular its intensity dependence has not been investigated.

In this work we study CL and PL of Yb^{3+}-Er^{3+} co-doped fluoride PbF_2 nanoparticles of 8 nm diameter with doping level up to 10 at% and active phonon energies below 250 cm^{-1}. Yb^{3+} is known to have strong infrared emission band about 1 μm wavelength and therefore might serve as infrared CL phosphor. Smaller portion of Er^{3+} ions was added to our samples since Er^{3+} emits two green PL bands and the ratio of these bands indicates the temperature rise in the emitting nanoparticles, see e.g. in [15,16]. Note, the temperature rise for few hundreds degrees Celsius is intrinsic for CL phosphors in cathode-ray tubes and it decreases efficiency of CL, e.g. in [17], therefore the knowledge of the temperature rise is important. The energy efficiency for CL has been estimated in the range from 400 to 1100 nm by comparison with CL intensity of etalon phosphor, as e.g. in [18].

We also have studied the intensity dependence of up- and down-conversion PL in these nanoparticles when pumped into absorption band of Yb^{3+} at about 980 nm. There is efficient energy transfer from Yb^{3+} to Er^{3+}, which allows to pump PL of Er^{3+} via Yb^{3+}, e.g. in [19,20]. Perhaps a largest to date up-conversion PL efficiency has been found, in particular, the sum efficiency of the red and green up-conversion PL bands of Er^{3+} became larger than efficiency of its down-conversion PL band at 1.55 μm, when normalized to one absorbed photon, at a pump power higher than 50 W/cm^2.

2. Experimental and results

The PbF_2 nanoparticles co-doped with Yb^{3+} and Er^{3+} has been prepared by the method proposed in [11] by chemical etching of the respective Yb^{3+}-Er^{3+} co-doped bulk glass-ceramic, which was prepared as in [21]. The transmission electron microscope (TEM) images of nanoparticles aggregates/nanopowder are shown in Figs. 1(a), 1(b), 1(c), 1(d). The nanoparticles are spherical and homogeneous in diameter, which is about 8 nm and their chemical formula is $(Yb\text{-}Er)_xPb_{1-x}F_{2+x}$, where $x = 0.29$, $Yb^{3+}/Er^{3+} = 6$, as identified by means of transmission electron microscope with attachment for energy dispersion X-ray spectroscopy (TEM EDX) at Laboratoire de Photonique et Nanostructure, Marcoussis, France, and at TEM EDX facility of Antwerpen University, Belgium.
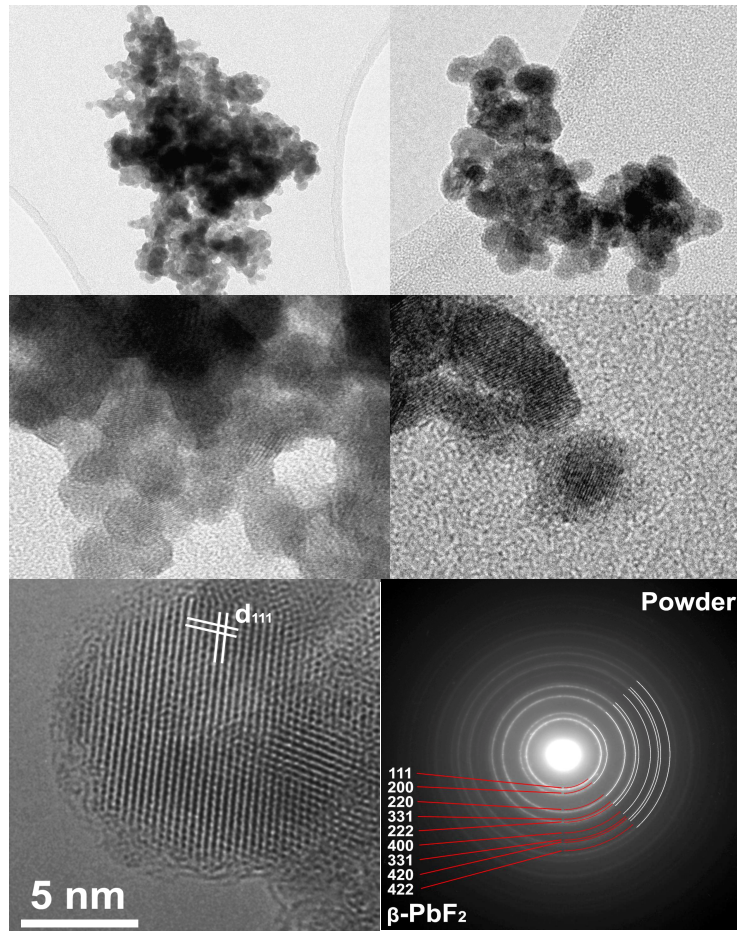

Fig. 1. (a,b,c,d) TEM images of nanoparticles with different spatial resolution. Black round spots of about 8 nm diameter are the nanoparticles comprising the aggregates/nanopowder. e) TEM image of single nanoparticle, where crystalline planes (1,1,1) of β-PbF_2 are indicated. f) Electron diffraction pattern taken from nanopowder, where the diffraction rings from certain planes of the β-PbF_2 are indicated.

Figures 1(e), 1(f) indicate that the structure of the nanoparticles is a face centered cubic structure of the classic substituted fluorite (or β-PbF_2 [21]), which is $(Yb\text{-}Er)_xPb_{1-x}F_{2+x}$, where $x = 0.29$ [20 and refs therein]. The lattice parameter of the nanoparticles, Figs. 1(e), 1(f), is slightly shorter than in β-PbF_2 due to smaller ionic radii of rare-earth ions compared to Pb^{2+}, as argued in [21]. When doing the TEM EDX experiments, we have noted that the fluorine ions tend to move away from the area irradiated by the electron beam due to high superionic

conductivity of the β-PbF$_2$ and negative charge of the electron beam. Therefore, the proportion of Yb, Er and Pb ions can be certainly found in TEM EDX experiments, while the proportion of registered F ions slightly depends on the parameters of the electron beam. As we have not found in EDX spectra any other elements apart from Yb^{3+} Er^{3+}, Pb^{2+} and F$^-$, the proportion of F$^-$ ions was estimated exactly by charge compensation criterion, which corresponds to the classic substituted fluorite (Yb-Er)$_x$Pb$_{1-x}$F$_{2+x}$, where x = 0.29. The solubility of the rare-earth dopants in this *stoichiometric* compound of *tveitite* type will be addressed in the end of Discussion section.

For measurement of CL, the nanopowder was placed on sample holder of scanning electron microscope (SEM) consisting of carbon membrane on copper grid. The SEM has an attachment to measure CL with CCD camera. The pieces of nanopowder were spread over areas of free carbon membrane and carbon membrane lying on Cu grid. Electron beam diameter on sample was 10 nm; exposure time to beam was 1 second. SEM was operating at 20 kV and 3 nA.

Figure 2 shows CL spectra of the nanoparticles spread over carbon membrane substrate (postsigned "C substrate", red curve) and over carbon membrane on copper grid (postsigned "Cu substrate", blue curve). Emission band of Yb^{3+} centered at about 1020 nm dominates the spectrum as expected due to higher concentration of Yb^{3+} ions and highest cross-section for this emission transition. Emission bands corresponding to Er^{3+} are postsigned in Fig. 2. The spectral response/sensitivity of the CCD detector was taken into account. Insert in Fig. 2 shows expanded range of visible PL corresponding to transitions of only Er^{3+}.

Here we see two green emission bands of Er^{3+} from 510 nm to 535 nm, and from 535 nm to 565 nm corresponding to the ^{2}H$_{11/2}$→^{4}I$_{15/2}$ and ^{4}S$_{3/2}$→^{4}I$_{15/2}$ transitions. The integral intensity ratio of these two bands is defined by the temperature T of the emitting sample, [15,16 and refs therein], according to Eq. (1):

$$\ln\left(\frac{I_H}{I_S}\right) = C - \frac{B}{T} \tag{1}$$

where I_H and I_S are intensity of the ^{2}H$_{11/2}$→^{4}I$_{15/2}$ and ^{4}S$_{3/2}$→^{4}I$_{15/2}$ emission bands, respectively, B and C are the constants [9,16 and refs therein]. The values of constants B and C for the studied PbF$_2$ nanopowder have been found by measuring intensity ratio I_H/I_S with varying sample temperature by means of cryostat, while PL was pumped by low intensity light into upper lying ^{4}F$_{3/2}$ level of Er^{3+} avoiding heating of the sample by pump beam, as shown in Fig. 3 in [9]. Using those values of B and C and intensity ratio of the ^{2}H$_{11/2}$→^{4}I$_{15/2}$ and ^{4}S$_{3/2}$→^{4}I$_{15/2}$ emission bands, a 800°C heating was calculated for the red curve in insert to Fig. 2, which corresponds to nanoparticles placed onto C membrane. On the other hand, for the blue curve in the same insert, the heating was only up to 400°C; this indicates importance of Cu metal with high thermal conductivity for more efficient heat transfer.

Since the electron beam can be focused into spot down to 10 nm, right in a *single* nanoparticle, this nanoparticle can be locally heated to the desired temperature (identified by ratio of green emission bands of Er^{3+}) and used, for example, for nano perforation of underlying thin metal film, which is otherwise impossible, i.e. by pure electron beam.

Most of emission bands seen in CL spectra of Fig. 2 are also observed in PL spectra in Fig. 4. In addition, some extra emission bands are detected in CL spectra of Fig. 2, which may correspond to emission from some upper lying levels of Er^{3+}, which is typical for CL since electron beam can excite any level of Er^{3+}. These extra emission bands may also come from unidentified impurities, i.e. from Eu^{3+}, which are unavoidable in rare-earth chemicals even of highest purity, such as we used (ErF$_3$ and YbF$_3$ of REacton grade, 99.99% purity, from Alfa Aesar). Also, Er^{3+} has emission band ^{4}I$_{9/2}$→^{4}I$_{15/2}$, which overlaps with ^{2}F$_{5/2}$→^{2}F$_{7/2}$ band of Yb^{3+} at about 1 μm, but that band of Er^{3+} is much weaker than Yb^{3+} band due to order of magnitude weaker oscillator strength and smaller doping level compared to Yb^{3+}.
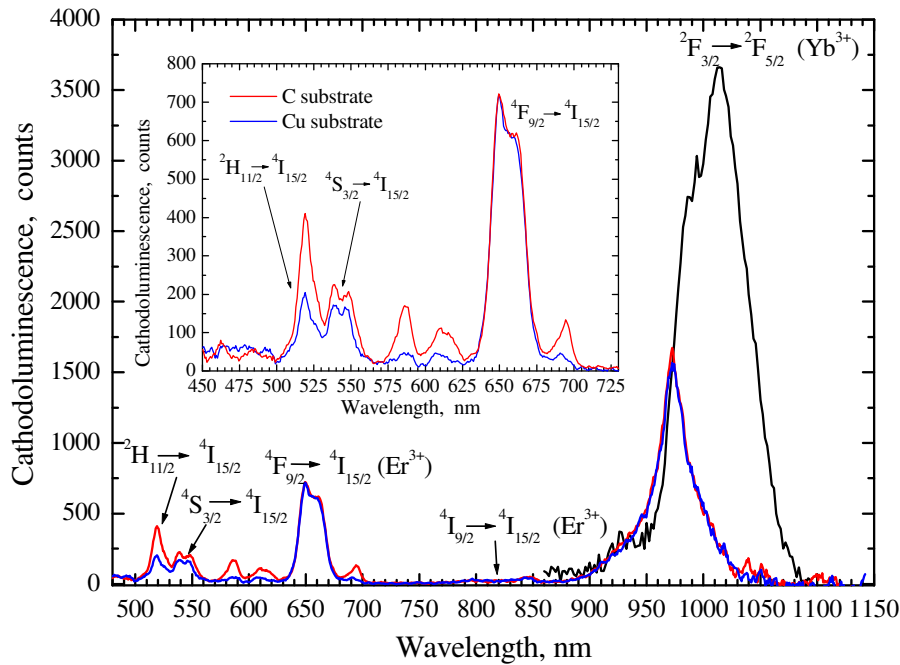
Fig. 2. Cathodoluminescence spectra of Yb^{3+}-Er^{3+} co-doped nanopowder normalized to emission band at 650 nm. Insert shows expanded area between 450 to 725 nm. CCD detector operates in spectral range between 450 to 1000 nm; therefore emission band of Yb^{3+} about 1000 nm is approximated above 1000 nm by the corresponding photoluminescence band (black curve) of the same nanoparticles excited via Er^{3+} co-dopant at 650 nm. Emission transitions are postsigned according to energy level diagram in Fig. 3.

Then we have estimated energy conversion efficiency for emission bands of CL. For this, first we have measured, in the same experimental conditions, CL spectrum from the reference aluminum film, for which the energy conversion efficiency spectrum was earlier defined in our laboratory using standard CL phosphors [17,18]. In our set-up, the CL is collected by parabolic mirror with 2π steradian solid angle, which assures that luminescence is collected in the same experimental conditions for the reference sample, and for the investigated sample. Then, we compared spectra from Fig. 2 with spectrum from this reference aluminum film and estimated the energy conversion efficiency for spectra of Fig. 2. The following values for energy conversion efficiency η were obtained for the blue curve in Fig. 2: for $^4S_{3/2} \rightarrow ^4I_{15/2}$ band of Er^{3+} $\eta = 2.09 \times 10^{-4}$, for $^4F_{9/2} \rightarrow ^4I_{15/2}$ band of Er^{3+} $\eta = 8.29 \times 10^{-4}$, and for $^2F_{5/2} \rightarrow ^2F_{7/2}$ band of Yb^{3+} $\eta = 4.05 \times 10^{-3}$, so that the total quantum yield of the visible emission bands of Er^{3+} and emission band of Yb^{3+} was about 6×10^{-3} or 0.6% which is perhaps the only available value to date for rare-earth dopants nanoparticles.

For measurement of PL, the nanopowder was placed and squeezed between two microscope slides, so that the thickness of nanopowder layer was several hundred microns. The nanopowder was then set onto a stage of CRAIC QDI 2010 microspectrophotometer, which allowed measuring the PL of the nanopowder via microscope. The PL was excited by the beam of 100 mW laser diode operating at 980 nm wavelength, and incident onto the nanopowder layer at the angle of 45°. The beam was focused with a laser collimator. The PL was simultaneously measured by two CCD cameras, which operate in the visible and near

infrared ranges of spectrum, respectively. The total spectral response of the microspectrophotometer was evaluated and taken into account.

Fig. 3. Energy level diagram of Yb^{3+} and Er^{3+}. The down-headed arrows indicate transitions postsigned in spectra of Figs. 2 and 4, respectively.

Figure 4 shows PL spectrum of the nanopowder pumped at indicated power of the 980 nm laser diode. The pumping was done mostly into absorption band $^2F_{7/2} \rightarrow {}^2F_{5/2}$ of Yb^{3+} and to the much lower degree into absorption band $^4I_{15/2} \rightarrow {}^4I_{9/2}$ of Er^{3+}, as can be seen in energy level diagram of Fig. 3. It is because the absorption cross-section of the former band of Yb^{3+} is 3.3 times larger than for the later band of Er^{3+}, and concentration of Yb^{3+} ions is 6 times larger than of Er^{3+} ions. The spectrum consists mainly of up-conversion PL bands centered at 650 and 550 nm (2-photon processes), 410 nm (3-photon process), e.g. in [22], and down-conversion PL band at 1530 nm (single-photon process), e.g. in [23]. The resonant luminescence band was obscured in this measurement due to strong background of scattered and reflected laser beam, while intensity of other luminescence bands were negligible compared to those shown in Fig. 4. The maximum pump intensity of 100 mW corresponds to the pump power density of about 80 W/cm^2, taking into account a radius of 200 μm of laser spot as shown in Fig. 5.

The bands corresponding to 2- and 3-photon up-conversion luminescence processes have been multiplied by factor of 2 and 3 in Fig. 4, respectively because emission of these bands occurs only when 2 and 3 photons are absorbed, respectively, while down-conversion band emits already after absorption of one photon [22]. Therefore, the quantum efficiency for up- and down-conversion luminescence bands *per one absorbed photon* can be compared from the spectra presented in Fig. 4.

At the lowest pump powers up to 5 mW, only the down-conversion PL band at 1.5 μm is present. With increasing the pump power, up-conversion PL bands emerge in the spectrum. At the highest pump power of 100 mW, the total energy flux in up-conversion PL bands becomes larger than for down-conversion PL band. In particular, at this pump power, the integrated area for the 410 nm band equals to 17200, for the 525 and 550 nm bands equals to 93213, and for the 650 nm band equals to 334070 resulting in total of 444483 square units, which is larger than the integrated area for the 1530 nm down-conversion PL band at 441914 square units.

While the down-conversion PL band shows a linear increase with pump power, typical of single photon processes, the up-conversion PL bands show super-linear dependence typical of 2 and 3-photon processes [19]. In particular, the red PL band at 660 nm has a power 1.8 on the Log-Log dependence of its intensity versus pump intensity, which is typical of 2-photon processes. The ratio of green PL bands $^2H_{11/2}{\rightarrow}^4I_{15/2}$ and $^4S_{3/2}{\rightarrow}^4I_{15/2}$ of Er^{3+} is small indicative of negligible temperature rise in the nanopowder, in particular perhaps due to heat release from the nanopowder into the holding microscope slides. Therefore, we assume that efficiency of up-conversion PL might be further increased should it be possible to further increase the pump power density.
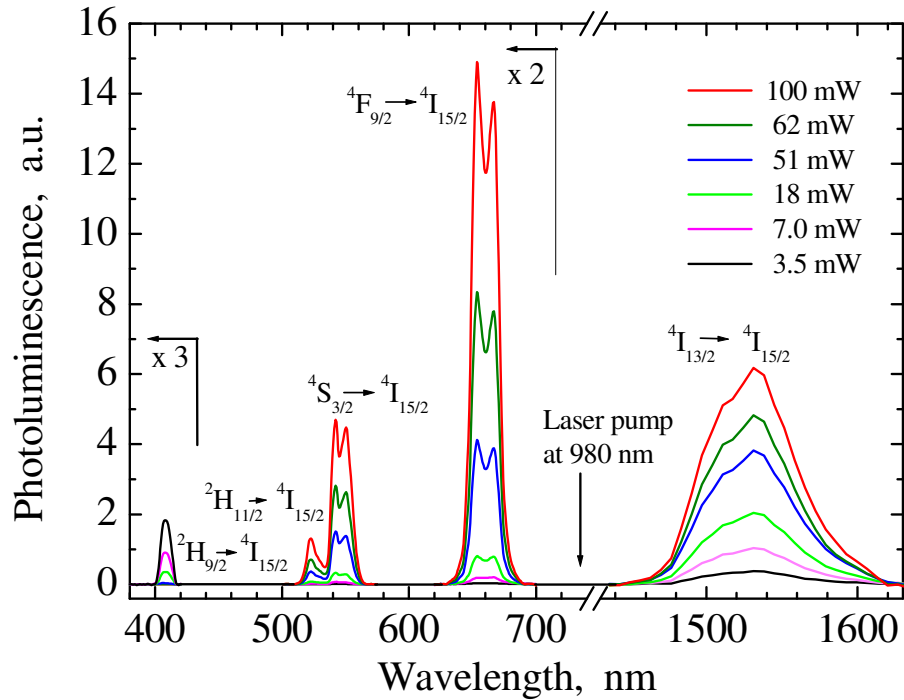
Fig. 4. Photoluminescence spectra of Yb^{3+}-Er^{3+} co-doped nanopowder excited at indicated pump powers and wavelength of the laser diode into absorption band $^2F_{7/2}{\rightarrow}^2F_{5/2}$ of Yb^{3+}. The up-conversion luminescence parts corresponding to 2- and 3-photon processes are multiplied by factor of 2 and 3, respectively.
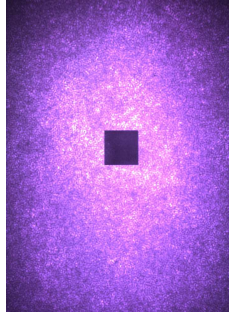
Fig. 5. Image of illuminated spot on the surface of Yb^{3+}-Er^{3+} co-doped nanopowder layer spread between microscope slides. Black square in the center has size 42×42 μm.

Figure 5 shows an image of photoluminescent spot on the surface of nanopowder, which was taken by a photocamera attached to the microspectrophotometer. The increase in intensity of the image in Fig. 5, from dark to bright, corresponds to strengthening of the intensity of the signal detected from the illuminated spot. We note the bright speckle dots in the image of Fig. 5, which are chaotically distributed across the illuminated spot. These chaotic distributed dots have also been seen by naked eye as green speckle dots on the surface of the nanopowder layer due to stronger green up-conversion luminescence signal. The random luminescent dots in the nanopowder have also been seen by the eye when scanning a focused beam of 2 mW laser diode across the surface of nanopowder, indicative that they are not due to unhomogeneity of laser beam, but rather are due to properties of the nanopowder. One of possibilities is that the random luminescent dots may be due to random nanolasing in the nanopowder, as observed e.g. in luminescent ZnO nanopowder [24], however possibility requires a separate investigation.

3. Discussion

Lanthanide dopants, such as Eu^{3+}, Tb^{3+} and Tm^{3+}are known as one of best red, green and blue CL phosphors, respectively [12–14,17]. On the other hand, infrared CL phosphors have not been widely investigated, since the main application of CL was in the visible fluorescent lamps and cathode ray tubes. It is seen from Fig. 2 and the above mentioned estimate of energy conversion efficiency of 0.5%, that Yb^{3+}-doped nanoparticle may be a good *infrared nano-scale CL phosphor* due to its high cross-section emission at about 1 μm. These nanoparticles can be also nanoscale light sources because a nano-scale size pump is available with the electron beam, which can be focused down to some nanometers, i.e. onto single nanoparticle [18]. To our knowledge, to date this is a first observation of CL from the lanthanide doped *nanoparticles*.

The current-to-light conversion efficiency of best CL phosphors is in the range of only several percents, therefore a substantial temperature rise up to hundreds degrees Celsius is inevitable in CL phosphors, e.g [17]. The temperature rise quenches CL [17]; therefore it is important to be aware of actual temperature of CL phosphor to optimize its operation. Here we showed that the temperature rise in CL phosphor can be estimated by its co-doping with smaller portion of Er^{3+} ions and measuring the ratio of two thermalised green emission bands of Er^{3+}.

The conversion efficiency in our case is lower than in commercial CL phosphors for visible range due to several reasons, which may be principally overcome: i) the heating of nanoparticles is stronger than in bulk materials due to lower heat release [9], resulting in stronger quenching of CL in nanoparticles ii) Yb may be intrinsically less efficient phosphor than the standard phosphors based on Eu and Tb iii) the surface of the nanoparticles can be contaminated with water and OH radial impurities which quench CL.

It is seen from Fig. 4 that Yb^{3+}-Er^{3+} co-doped nanoparticles can also serve for efficient light frequency up-conversion when the pump power exceeds about 10 W/cm^2. We could not measure the resonant luminescence of Yb^{3+}-Er^{3+} co-doped nanopowder at about 1000 nm due

to strong Rayleigh scattering and reflection of pump laser beam typical of nanopowders, see break in Fig. 4.. However, it was possible to measure the resonant emission band and the full emission spectrum of the respective Yb^{3+}-Er^{3+} co-doped bulk *transparent* glass-ceramics, where the same Yb^{3+}-Er^{3+} co-doped nanoparticles are dispersed in glassy matrix [11,20–23] and Rayleigh scattering and reflection for the pump laser beam are essentially weaker. In the latter case, the measurement was done with a grating dispersion spectrometer and, sequentially, with several photodetectors, normalizing the respective sequential spectra to the overlapping emission bands, while the spectral response of the spectrometer was taken into account, as in Ref [22,25]. The spectrum of bulk glass-ceramics is shown in Fig. 6, when pump power was 50 W/cm^2. When we compare the spectrum for bulk glass-ceramics in Fig. 6 and the respective spectrum of nanopowder at the same pump power in Fig. 4 (dark green curve), we see that these spectra are very similar, apart from the resonance emission band, which is absent in the spectrum of nanopowder as it was discussed above. Thus, the resonance emission band is assumed to be the same in bulk glass-ceramics and in nanopowder, as well as the remaining parts of their spectra.
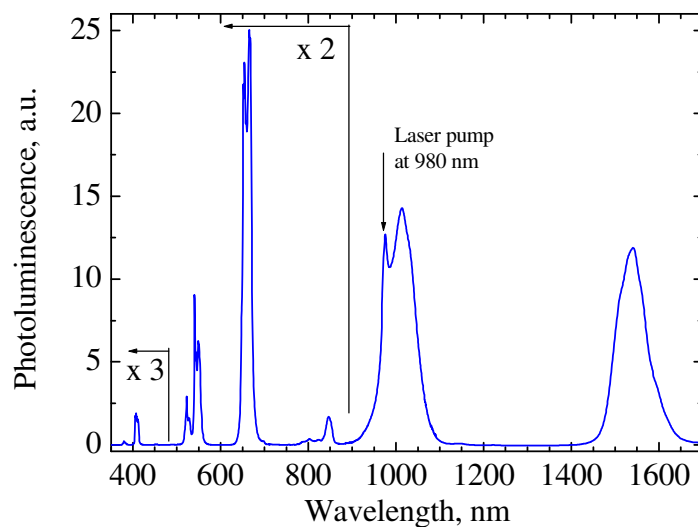

Fig. 6. Photoluminescence spectra of bulk Yb^{3+}-Er^{3+} co-doped glass-ceramics excited at 50 W/cm^2 pump power and wavelength 980 nm of the laser diode into absorption band $^2F_{7/2} \rightarrow {}^2F_{5/2}$ of Yb^{3+}. The up-conversion luminescence parts corresponding to 2- and 3-photon processes are multiplied by factor of 2 and 3, respectively.

It is seen in Figs. 4 and 6 that the total photon flux in up-conversion PL bands (at pump power above 50 W/cm^2) *per one absorbed photon* overcome the photon flux in the down-conversion PL band at 1550 nm and resonant PL band at 1020 nm. This indicates a very high conversion efficiency, or quantum yield, for the up-conversion PL at high pump power density. For example, at pump power of 50 W/cm^2, as seen in Figs. 4 and 6, the total photon flux in up-conversion PL bands comprises more than 25% of the total PL flux. Here we note that the value of up-conversion yield higher than 20% at pump power density about 50 W/cm^2 has been estimated by Rodriguez et al in [22] for the bulk sample of single Er^{3+}-doped glass-ceramics based on analysis of its full PL spectrum and pump power dependence of the resonance PL band. Now we see that in Yb^{3+}–Er^{3+} co-doped bulk glass-ceramics (Fig. 6) and nanoparticles (Fig. 4) the quantum yield for up-conversion PL is higher than in Er^{3+} single doped sample [22]. This may be because the Er^{3+} dopant is only a minor dopant in Yb^{3+}-Er^{3+} co-doped samples in this paper, its concentration is 7 times smaller than it was in Ref [22].

This results in suppression of depopulation of excited Er^{3+} levels due to the cross-relaxation process [22] and suppression of heating loss due to non-radiative decay of excited levels of Er^{3+} [9], because the excited electrons are kept the most of time on the excited level of Yb^{3+}, which does not depopulate non-radiatively. Therefore, we conclude that the total quantum yield for the up-conversion red and green PL bands in Fig. 4 exceeds 20% at pump power density above 50 W/cm^2.

To explain the reasons for high quantum efficiency of CL and up-conversion PL, we note that the probability $W_{nr}^n(T)$ for non-radiative/phonon assisted decay of the rare-earth energy level with simultaneous emission of n phonons at temperature T is defined by Eq. (2)

$$\frac{1}{\tau_{\exp}} = W_{nr}^n(T) + \frac{1}{\tau_{rad}}$$
(2)

where $\tau_{\exp}$ is the experimental lifetime and τ_{rad} is the radiative lifetime of the level. It is seen from Eq. (2) that the $W_{nr}^n(T)$ term should be suppressed to support the radiative decay. On the other hand, $W_{nr}^n(T)$ is also defined by Eq. (3):

$$W_{nr}^n(T) = W_{nr}^n(0) \times \left[1 - \exp\left(\frac{-\hbar\omega}{kT} \right) \right]^{-n}$$
(3)

where n is the number of phonons $\hbar\omega$, which bridges the gap between the emitting level and the nearest lower lying level. Thus, $W_{nr}^n(T)$ increases drastically with $\hbar\omega$ (or decreases drastically with n) and therefore, for efficient radiative decay/emission of the emitting level, according to Eqs. (2) and (3), $\hbar\omega$ should be as small as possible, i.e. substantially smaller than 500 cm^{-1}. The nanoparticles proposed in this paper offers maximal phonon energy coupled to the rare-earth dopant as small as 250 cm^{-1}, which therefore ensures small values of the non-radiative decays $W_{nr}^n(T)$ and consequently, high values of radiative decays.

The high, up to 10 at.%, doping level of these nanoparticles, as follows from the chemical formula of the nanoparticles $(Yb\text{-}Er)_x Pb_{1-x} F_{2+x}$, where $x = 0.29$ (Fig. 1), assures efficient energy transfer between the Yb^{3+} and Er^{3+} co-dopants, which defines the mechanism for the up-conversion co-operative luminescence at the high doping level, e.g. in [19,22]. In this respect, the homogeneity of the dispersion of Yb and Er ions in the PbF_2 lattice is important. The $Re_x Pb_{1-x} F_{2+x}$ is known as a stoichiometric compound, where Re is a rare-earth atom or Y atom, $x = 0.29$ and Ca may substitute for Pb. This stoichiometric compound is called *tveitite* and rare-earth ions dissolve in this compound without clustering, e.g. in [26,27 and refs therein]. Apparently, the high luminescence yield reported in this work proves high solubility/dispersion of the rare-earth dopants in tveitite structure because the clustering of the dopants could result in the concentration quenching of luminescence.

4. Conclusion

We have shown results which indicate that the PbF_2 nanoparticles can be doped with rare-earth ions, such as Yb^{3+} and Er^{3+}, to very high doping level of 10 at.%, and their luminescence is still not concentration quenched. The high quantum yields for the cathodoluminescence and up-conversion photoluminescence in these nanoparticles are due to that high doping level and very low active phonon energy of 250 cm^{-1}, of the PbF_2 host, which suggest that these nanoparticles provide perhaps the highest available quantum yields for cathodo- and photoluminescence of rare-earth dopants.

Acknowledgement